



Development of polyaniline-derived carbon materials for applications in Direct Ethanol Fuel Cells

María Florencia Azcoaga Chort*, Virginia Inés Rodríguez, Natalia Soledad Veizaga.

Instituto de Investigaciones en Catálisis y Petroquímica (INCAPE), CCT CONICET, Ruta Nacional 168 Km 0, Paraje "El Pozo", CP: 3000, Santa Fe, Argentina. *Email: fazcoaga@fiq.unl.edu.ar

Resumo/Abstract

RESUMO - Foram sintetizados três materiais — PANI, PANI₈₀-NT₂₀ e PANI₅₀-NT₅₀ — com o objetivo de utilizá-los como suportes em eletrocatalisadores anódicos. Catalisadores mono- e bimetálicos de Pt e PtRe(3) foram preparados utilizando o método do poliol. Os suportes e os catalisadores foram caracterizados por meio de fisissorção de N₂, termogravimetria, difração de raios X, microscopia eletrônica de transmissão, dessorção e redução em temperatura programada, quimissorção de H₂ e reaçãoteste de hidrogenação de benzeno. Além disso, os catalisadores foram avaliados eletroquimicamente por voltametria cíclica, cronoamperometria e stripping de CO. Por fim, foram realizados ensaios em uma célula protótipo de etanol direto para avaliar o desempenho dos catalisadores em condições próximas às reais. O catalisador bimetálico PtRe(3)/PANI₅₀-NT₅₀ apresentou o melhor desempenho na semicélula, alcançando uma área eletroquimicamente ativa de 60 m² gPt⁻¹. O potencial de início para a oxidação do etanol foi de 220 mV (vs Ag/AgCl), e a corrente máxima de pico anódico atingiu 297 mA mgPt⁻¹. Além disso, esse mesmo catalisador apresentou o melhor desempenho na célula protótipo, alcançando valores de tensão em circuito aberto e densidade de potência de 496 mV e 3,0 mW cm⁻², respectivamente.

Palavras-chave: PANI, PANI-NT, PtRe, eletrocatalisadores, DEFC.

ABSTRACT - Three materials —PANI, PANI₈₀-NT₂₀, and PANI₅₀-NT₅₀ — were synthesized with the aim of using them as supports in anodic electrocatalysts. Mono- and bimetallic catalysts of Pt and PtRe(3) were prepared using the polyol method. Both the supports and catalysts were characterized by N₂ physisorption, thermogravimetric analysis, X-ray diffraction, transmission electron microscopy, temperature-programmed desorption, temperature-programmed reduction, H₂ chemisorption, and benzene hydrogenation test reaction. Additionally, the catalysts were electrochemically evaluated using cyclic voltammetry, chronoamperometry, and CO stripping. Performance tests were also conducted in a prototype direct ethanol fuel cell to assess the behavior of the catalysts under conditions close to real operation. The bimetallic catalyst PtRe(3)/PANI₅₀-NT₅₀ exhibited the best performance in the three-electrode half-cell, achieving an electrochemically active surface area of 60 m² gPt⁻¹. Furthermore, it showed an onset potential for ethanol oxidation of 220 mV (vs Ag/AgCl) and a maximum anodic peak current of 297 mA mgPt⁻¹. This catalyst also demonstrated the highest performance in the prototype cell, reaching open-circuit voltage and power density values of 496 mV and 3,0 mW cm⁻², respectively.

Keywords: PANI, PANI-NT, PtRe, electrocatalysts, DEFC.

Introduction

The increasing environmental pollution, primarily driven by the excessive use of non-renewable energy sources, has prompted the development of sustainable technologies for clean energy generation. In this context, fuel cells have emerged as a promising alternative for transportation and portable device applications. Among them, direct ethanol fuel cells (DEFCs) stand out due to their ability to operate at low temperatures, eliminate the need for fuel reforming and hydrogen storage, and use liquid ethanol as a fuel.

To enhance their performance, various materials have been investigated as catalytic supports, with carbon-based materials (such as activated fibers, nanotubes, and mesoporous carbons) being particularly noteworthy due to their favorable physicochemical and structural properties (1). Conductive polymers, such as polyaniline, have also been explored, as they exhibit good stability, redox behavior, and high conductivity. The combination of polyaniline with carbon nanotubes in composite materials has shown significant improvements in mechanical and electrical properties (2).

Regarding catalysts, platinum (Pt) is widely used due to its efficiency in alcohol oxidation, although it is susceptible to deactivation through CO poisoning. To mitigate this effect, bimetallic systems incorporating metals such as Ru, Sn, Mo, Rh, and Ni have been proposed. Among these, rhenium (Re) has proven particularly effective in facilitating C–C bond cleavage at low temperatures, a key step for the complete oxidation of ethanol (3).

Therefore, the main objective of this work is to investigate the effect of incorporating rhenium (Re) into



platinum (Pt)-based catalysts supported on carbonized polyaniline (PANI), carbon nanotubes (NT), and PANI–NT composites for application in the electrooxidation of ethanol in DEFCs. The study aims to elucidate the structural, physicochemical, and electrochemical properties of these catalytic systems, with particular emphasis on the role of the support and the synergistic interactions between the metals. The key contribution of this work lies in demonstrating how the use of hybrid PANI–NT supports, combined with Re as a promoter, enhances catalytic activity and stability, providing valuable insights for the development of more efficient and sustainable electrocatalysts for DEFC applications.

Experimental

Materials.

The following reagents were used: pure aniline (Biopack), ammonium persulfate (APS, Biopack), hydrochloric acid (Cicarelli), ammonium hydroxide (Cicarelli), absolute ethanol (Biopack), ethylene glycol (EG, Cicarelli), and distilled water. Additionally, purified multiwalled carbon nanotubes (NT), provided by Sunnano, were employed. As metallic precursors, chloroplatinic acid and perrhenic acid (both from Alfa Products) were used.

Support Synthesis.

Polyaniline was synthesized via in situ polymerization. A 1 M HCl solution containing aniline and APS was prepared and stirred in an ice bath for 2 h. The resulting product was filtered and washed with 1 M HCl followed by abundant distilled water. It was then dried at 70 °C for 48 h. Subsequently, the material was treated with NH₄OH for 24 h, filtered, washed thoroughly with distilled water, and dried at 70 °C for another 48 h (4).

The synthesis of polyaniline in the presence of NT (in 80:20 and 50:50 mass ratios) also followed the in situ polymerization method. A small portion of the 1 M HCl solution was used to wet the NT, which were then sonicated for 1 h. In another portion of 1 M HCl, the corresponding amount of aniline was diluted, the NT were added, and the mixture was sonicated for 5 min. This mixture was stirred in an ice bath. Separately, APS was dissolved in another portion of 1 M HCl and added dropwise to the aniline-NT mixture. After complete homogenization, polymerization was carried out for 2 h in an ice bath. The resulting product was filtered and washed with 1 M ethanol and abundant distilled water until the pH reached 5. It was then dried at 70 °C for 48 h, treated with NH₄OH for 24 h, filtered, washed thoroughly with water, and dried again at 70 °C for 48 h (1).

The final materials were obtained by thermal treatment at 800 °C for 2 h under a nitrogen atmosphere, using a heating rate of 5 °C min⁻¹. The resulting supports are referred to as PANI, PANI₈₀-NT₂₀, and PANI₅₀-NT₅₀.



Catalyst Synthesis.

The catalysts were synthesized using the polyol method. The respective supports were dispersed in a H₂O:EG solution (25:75 %v/v) and sonicated for 30 min. The required amounts of Pt and Re precursors were then added. The mixture was refluxed for 2 h, followed by filtration, washing with distilled water, and drying at 110 °C for 2 h (5). The nominal Pt and Re loadings were 20 %wt. and 3 %wt., respectively. For comparison purposes, Pt and PtRe(3) catalysts supported on NT were also prepared.

Characterization Methods.

The supports and catalysts were characterized using various techniques: N₂ physisorption, thermogravimetric analysis (TGA), temperature-programmed desorption (TPD), temperature-programmed reduction (TPR), hydrogen chemisorption, benzene hydrogenation reaction, X-ray diffraction (XRD), transmission electron microscopy (TEM), cyclic voltammetry (CV), chronoamperometry, CO stripping, and performance evaluation in a prototype direct ethanol fuel cell.

Results and Discussion

In the case of multiwalled carbon nanotubes, the isotherm corresponds to a type III profile within the range of moderate relative pressures (P/P⁰). For PANI and the composite supports (PANI₈₀-NT₂₀ and PANI₅₀-NT₅₀), the isotherms exhibit a type I shape at low P/P⁰ values, transitioning to a type II-like shape at intermediate pressures. Additionally, these isotherms display an H4-type hysteresis loop, whereas no hysteresis is observed for the NT. The specific surface areas obtained were 179, 430, 318, and 187 m² g⁻¹ for NT, PANI, PANI₈₀-NT₂₀, and PANI₅₀-NT₅₀, respectively. These values are consistent with those reported in the literature for both pure and composite supports.

Regarding the thermogravimetric measurements, a negligible mass loss (less than 0.5% at the end of the analysis) was observed for the carbon nanotubes (NT). In contrast, PANI and the composite supports exhibited a slight decrease in mass (less than 2.5% in all three cases) in the 25–150 °C range, which can be attributed to the evaporation of water from the samples. Subsequently, a more pronounced mass loss was observed between 150 and 850 °C, likely due to the thermal decomposition of PANI and/or the carbonization of chemical intermediates (6). For the composite supports, the final residue at 900 °C increased with the amount of NT incorporated into the material. This result may be related to the formation of a more ordered structure promoted by the presence of NT during the synthesis process (7).



Analysis of the TPD profiles (Figure 1a) shows that the NT exhibit no desorption peaks, indicating the absence of surface functional groups. In contrast, the TPD curve for PANI displays desorption peaks beginning at approximately 250 °C. This behavior is attributed to the presence of surface functional groups—such as carboxylic acids, lactones, anhydrides, phenols, and ethers—which are released in the form of CO and CO₂. For the composite supports, the presence of functional groups is more pronounced in the material with a higher PANI content, specifically PANI₈₀-NT₂₀. Regarding the TPR profiles (Figure 1b), the NT show no hydrogen consumption peaks, which is consistent with the literature and the TPD results. On the other hand, the TPR profile of PANI displays a peak at high temperatures, which may be related to surface functional groups, depletion of the support, or thermal decomposition of the material. Moreover, hydrogen consumption at elevated temperatures could also be attributed to the presence of specific functional groups such as HCN, NO, and N₂ (8).

The chemisorptive capacities of the mono- and bimetallic catalysts supported on NT, PANI, PANI₈₀-NT₂₀, and PANI₅₀-NT₅₀ are presented in Table 1. The values obtained for the bimetallic catalysts are lower than those of their corresponding monometallic counterparts, suggesting a possible interaction between the metals (Pt and Re) (9).

Table 1. Values of chemisorptive capacity (H), activation energy (E_{aBz}) , and initial velocity (R_{Bz}^0) for the benzene hydrogenation reaction of Pt and PtRe(3) catalysts supported on NT, PANI, PANI₈₀-NT₂₀ and PANI₅₀-NT₅₀.

Support	Catalyst	H (µmol g _{cat} -1)	E _{aBz} (kcal mol ⁻¹)	R_{Bz}^{0} (mol h ⁻¹ gpt ⁻¹)
NT	Pt	242	7.3	3.4
	PtRe(3)	225	11.1	4.3
PANI	Pt	120	20.5	1.1
	PtRe(3)	77	13.1	1.2
PANI ₈₀ - NT ₂₀	Pt	134	15.1	3.0
	PtRe(3)	121	14.0	2.1
PANI ₅₀ - NT ₅₀	Pt	170	9.8	3.7
	PtRe(3)	123	10.5	3.4

The results for the activation energy (E_{aBz}) and the initial rate of the benzene hydrogenation reaction (R_{Bz}^0) are summarized in Table 1. In the case of the PtRe(3)/NT catalyst, both parameters increase (by 52% and 26%, respectively) compared to those observed for Pt/NT, indicating that there are no geometric hindrances or site-blocking effects from Re. Moreover, these results suggest electronic modifications of the Pt active sites due to the addition of the second metal. For the PtRe(3)/PANI catalyst, a 35% decrease in E_{aBz} is observed compared to its monometallic counterpart. However, the R_{Bz}^0 value remains



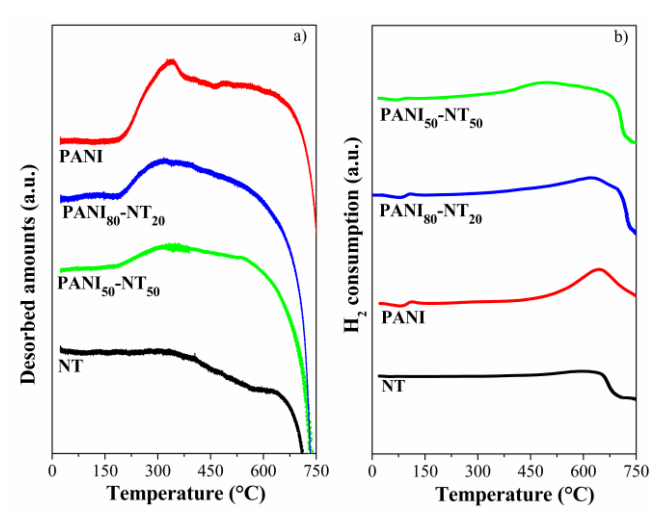


Figure 1. TPD (a) and TPR (b) curves of NT, PANI, PANI₈₀-NT₂₀, and PANI₅₀-NT₅₀ supports.

nearly unchanged, with a variation of less than 10%. The observed changes in activation energy may indicate electronic modifications resulting from the addition of Re, as well as metal–support interactions arising from the presence of surface functional groups on the support. The bimetallic catalysts supported on PANI₈₀-NT₂₀ and PANI₅₀-NT₅₀ show variations in E_{aBz} relative to their respective monometallic analogues, in line with the composition of each pure support. These findings may point to electronic alterations of the Pt sites induced by the presence of the promoter. On the other hand, R_{Bz}^0 values decrease for both composite supports in comparison with their monometallic counterparts, which may indicate a slight dilution or blocking effect.

Regarding the temperature-programmed reduction (TPR) results of the catalysts, no significant peaks were identified in the typical reduction regions for Pt or Re (100–200 °C and 350–450 °C, respectively). This observation, consistent with previous findings, suggests that Pt is predominantly present in its metallic state (Pt^0) (10). On the other hand, the results obtained through TPR on the reducibility of Re show that this metal would be mostly in the metallic state (Re⁰). Due to the complex reducibility of Re, its oxidation state could not be accurately determined by this technique alone. For this reason, a complementary analysis by X-ray photoelectron spectroscopy was performed. The results obtained by this technique show that Re is mostly in the oxidized state (Re⁶⁺). This is in contrast to what was found by TPR, so that no conclusive results could be obtained regarding the oxidation state of Re.

The lattice parameter and average crystallite size values were calculated from XRD data using the Pt (220) diffraction peak. In all cases, the variations in lattice parameters of the bimetallic catalysts compared to their corresponding monometallic counterparts were negligible





Table 2. Values of ethanol oxidation onset potential ($E_{EtOH,ONSET}$) and maximum anodic peak current (I_a) obtained by CV, and electrochemically active specific surface area (ECSA) and CO oxidation onset potential ($E_{CO,ONSET}$) obtained by CO stripping, of Pt and PtRe(3) catalysts supported on NT, PANI, PANI₈₀-NT₂₀, and PANI₅₀-NT₅₀.

Support	Catalyst	E _{EtOH,ONSET} (mV vs Ag/AgCl)	I _a (mA mgPt ⁻¹)	ECSA (m ² gPt ⁻¹)	E _{CO,ONSET} (mV vs Ag/AgCl)
NT	Pt	345	179	32	522
	PtRe(3)	260	267	52	500
PANI	Pt	434	43	20	384
	PtRe(3)	440	64	35	467
PANI ₈₀ -NT ₂₀	Pt	472	84	25	501
	PtRe(3)	236	171	46	279
PANI ₅₀ -NT ₅₀	Pt	321	199	41	395
	PtRe(3)	220	297	60	336

or absent. Considering that the atomic radii of Pt and Re are similar, it is difficult to conclude the incorporation of Re atoms into the Pt crystalline structure. Furthermore, variations in the supports did not lead to significant changes in these parameters. On the other hand, the average

crystallite size values showed no substantial differences between the bimetallic and monometallic catalysts.

TEM micrographs (Figure 2) revealed morphological differences among the pure supports. The characteristic tubular structure of the NT was distinctly observed, whereas no well-defined morphology was evident for PANI. Regarding the hybrid supports, PANI₈₀-NT₂₀ exhibited a morphology similar to that of PANI. In contrast, PANI₅₀-NT₅₀ displayed a more balanced combination of the morphologies of the pure supports, with visible tubular structures corresponding to NT and irregular growths around or near the nanotubes, without a defined shape, attributed to PANI. Metallic particles were found to be homogeneously distributed, and these observations are consistent with those reported in previous sections. As for the average particle diameter determined by this technique, the smallest value corresponded to the catalyst supported on NT, whereas the largest was found for the catalyst supported on PANI. The values obtained for the bimetallic catalysts supported on PANI₈₀-NT₂₀ and PANI₅₀-NT₅₀ did not follow the trend based on the proportions of the pure supports. Nevertheless, these results are in good agreement with the crystallite size values obtained from XRD analysis.

Table 2 presents the cyclic voltammetry results. Regardless of the support, the anodic scan peaks of the bimetallic catalysts are higher than those of their monometallic counterparts, indicating higher anodic currents and, therefore, improved electrocatalytic performance. Concerning $E_{\text{EtOH,ONSET}}$ values, the addition of Re leads to a significant decrease in most cases, which can be attributed to metal–metal interactions (11).

A comparison of the performance of mono- and bimetallic catalysts supported on different materials shows that

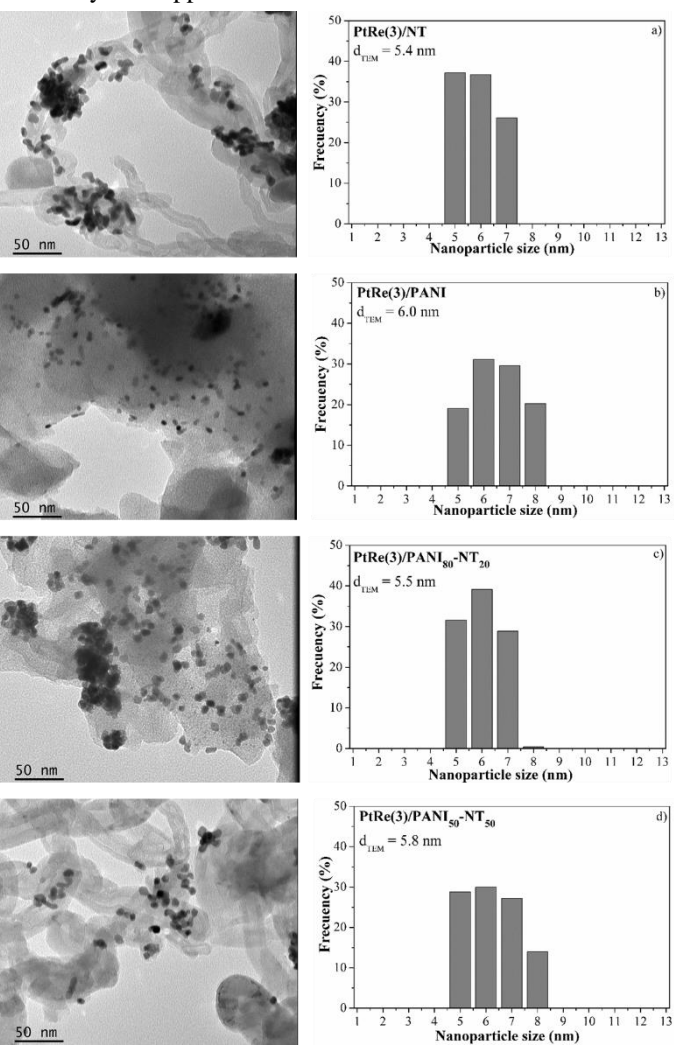


Figure 2. Micrographs and particle size distributions (a-d) obtained by TEM for PtRe(3) bimetallic catalysts supported on NT, PANI, PANI₈₀-NT₂₀ and PANI₅₀-NT₅₀.



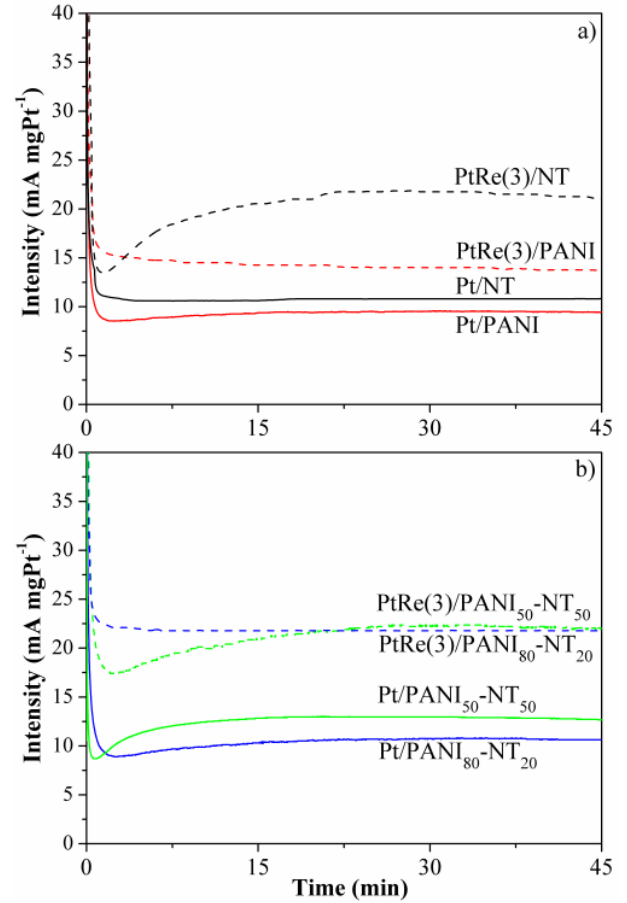


Figure 3. Chronoamperometric curves of Pt and PtRe(3) catalysts supported on a) NT and PANI and b) PANI₅₀-NT₅₀ and PANI₈₀-NT₂₀.

incorporating NT during the synthesis of PANI improves ethanol oxidation performance. PANI alone exhibits limited activity for the studied reaction, while NT display moderate behavior. Their combination during synthesis leads to a more ordered structure that generates a synergistic effect (8), enhancing catalytic activity. Moreover, the presence of functional groups introduced by PANI in the composite supports promotes electronic interactions at the metal–support interface, contributing positively to the electrochemical performance of the catalysts (12).

Table 2 also summarizes the electrochemically active surface area (ECSA) and CO oxidation onset potential (E_{CO,ONSET}) values obtained through CO stripping. In comparison, E_{CO,ONSET} values for the bimetallic catalysts were lower than those of the corresponding monometallic catalysts, with the exception of PtRe(3)/PANI, thereby highlighting a promotional effect of Re on Pt. Furthermore, when evaluating the ECSA of bimetallic catalysts versus their monometallic analogues, the addition of Re consistently led to an increase in ECSA, regardless of the support used. This phenomenon may also be attributed to metal—metal interactions. In addition, a comparative



analysis of PANI and NT supports shows that PANI has a smaller integrated area under the curve, implying a lower exposed Pt area available for the reaction. Conversely, the composite supports exhibit superior performance compared to PANI alone, with further improvements observed as the NT content increases.

The chronoamperometric curves (Figure 3) exhibit an initial period characterized by a rapid current decay, followed by a gradual decrease until a steady-state value is reached. For all supports, the bimetallic catalysts (with a Re loading of 3 %wt.) achieved higher steady-state current densities compared to their monometallic counterparts,

Figure 4a and 4b present the polarization and power density curves at 60 °C for the Pt and PtRe(3) catalysts supported on NT, PANI₈₀-NT₂₀, and PANI₅₀-NT₅₀. The polarization curves exhibited a sharp drop in potential at low current densities, attributed to activation losses. At higher current densities, a more gradual potential decline was observed, corresponding to ohmic losses. The open-circuit voltage (OCV) values for the analyzed catalysts were 457, 332, 465, 488, 367, and 496 mV for Pt/NT, Pt/PANI₈₀-NT₂₀, Pt/PANI₅₀-NT₅₀, PtRe(3)/NT, PtRe(3)/PANI₈₀-NT₂₀, and PtRe(3)/PANI₅₀-NT₅₀, respectively. The highest OCV values were obtained with the bimetallic catalysts,

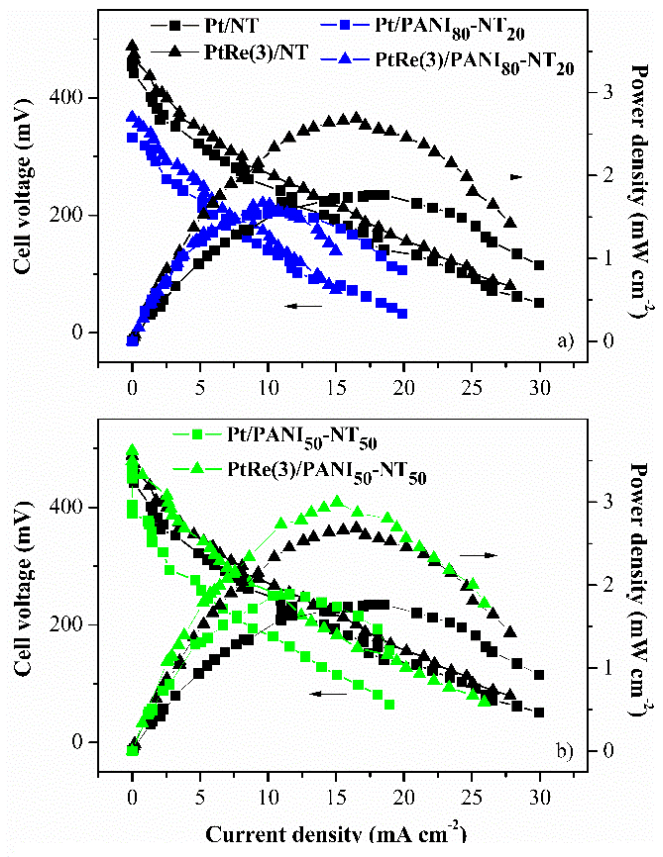


Figure 4. Polarization and power density curves of Pt and PtRe(3) catalysts on NT compared to those supported on PANI₈₀-NT₂₀ (a) and PANI₅₀-NT₅₀ (b).



confirming the results observed in the three-electrode cell and highlighting the synergistic interaction between the metals. Regarding the power density values, the addition of Re was found to enhance performance, yielding higher values of this parameter. The power density values for the analyzed catalysts were 1.8, 1.5, 2.7, 1.9, 1.7, and 3.0 mW cm⁻² for Pt/NT, Pt/PANI₈₀-NT₂₀, Pt/PANI₅₀-NT₅₀, PtRe(3)/PANI₈₀-NT₂₀, and PtRe(3)/PANI₅₀-NT₅₀, respectively. The best performance was achieved by the catalyst supported on PANI₅₀-NT₅₀, in agreement with the OCV results and polarization curves. The results obtained in the prototype cell are consistent with those observed in the three-electrode cell, where the best performance was also recorded for the catalyst supported on the combined PANI₅₀-NT₅₀ material.

Conclusions

PANI, PANI₈₀-NT₂₀, and PANI₅₀-NT₅₀ were synthesized to be used as supports in anode electrocatalysts for direct ethanol fuel cells. Pt and PtRe(3) catalysts were prepared through the liquid-phase reduction method, using ethylene glycol as the reducing agent. Textural analyses indicated that the synthesized materials presented adequate microand mesoporosity. In addition, it was observed that increasing NT in the combined supports increases the stability and electrocatalytic performance, suggesting a positive synergy in the PANI₅₀-NT₅₀ support. Results obtained from TGA, TPD, and TPR analyses indicated the presence of functional groups in PANI and the composite supports. The average crystallite and particle size values, obtained by XRD and TEM, respectively, did not show significant variations regardless of the support analyzed.

physicochemical Furthermore, based on the characterization of the catalysts, behaviors consistent with metal-metal and metal-support interactions were observed. Electrochemical evaluations using cyclic voltammetry, chronoamperometry, and CO stripping revealed that the bimetallic catalyst PtRe(3)/PANI₅₀-NT₅₀ exhibited the best electrochemical performance. This catalyst achieved an electrochemically active surface area of 60 m² gPt⁻¹, approximately 48% higher than that of the corresponding monometallic catalyst. In addition, the onset potential for ethanol oxidation and the maximum anodic peak current were 220 mV and 297 mA mgPt⁻¹, respectively. Regarding performance in the prototype cell, this catalyst also showed the best results, reaching open-circuit voltage and power density values of 496 mV and 3.0 mW cm⁻², respectively.

Acknowledgements

The authors gratefully acknowledge the support of the Universidad Nacional del Litoral and CONICET.



References

- A. Roy, A. Ray, P. Sadhukhan, K. Naskar, G. Lal, R. Bhar, C. Sinha, S. Das, Synth. Met. 2018, 245, 182–189.
- S. Ghatak, G. Chakraborty, A.K. Meikap, T. Woods, R. Babu, W.J. Blau, J. Appl. Polym. Sci. 2011, 119, 1016–1025.
- 3. J. Tayal, B. Rawat, S. Basu, Int. J. Hydrogen Energy **2012**, 37, 4597–4605.
- D. Salinas-Torres, J.M. Sieben, D. Lozano-Castello, E. Morallón, M. Burghammer, C. Riekel, D. Cazorla-Amorós, Carbon N. Y. 2012, 50, 1051–1056.
- E. V. Spinacé, R.R. Dias, M. Brandalise, M. Linardi, A.O. Neto, Ionics (Kiel). 2010, 16, 91–95.
- S. Bhadra, D. Khastgir, Polym. Deg. Stab. 2008, 93, 1094–1099.
- 7. T. David, J.K. Mathad, T. Padmavathi, A. Vanaja, Polymer **2014**, 55, 5665–5672.
- 8. H. Tang, M. Xiang, B. Xu, Y. Li, W. Han, Z. Liu, Chem. Res. Chinese U. **2018**, 34, 1004–1008.
- 9. B.H. Isaacs, E.E. Petersen, J. Catal. 1984, 85, 8-15.
- V.I. Rodríguez, N.S. Veizaga, S.R. de Miguel, J. Electrochem. Soc. 2017, 164, F1524–F1533.
- 11. A.K. Choudhary, H. Pramanik, Int. J. Hydrogen Energy. **2020**, 45, 13300–13321.
- 12. V. Comignani, J.M. Sieben, M.D. Sanchez, M.M.E. Duarte, Int. J.Hydrogen Energy. **2017**, 42, 24785–24796.